Geophysical Research Letters

RESEARCH LETTER
10.1029/2018GL081636

Attenuation of Storm Surges by Coastal Mangroves

J. M. Montgomery[1], K. R. Bryan[1], J. C. Mullarney[1], and E. M. Horstman[1,2]

[1]School of Science, Faculty of Science and Engineering, University of Waikato, Hamilton, New Zealand, [2]Water Engineering and Management, Faculty of Engineering Technology, University of Twente, Enschede, Netherlands

Key Points:
- An analytic solution is developed to describe storm surge propagation through coastal mangroves
- The water storage capacity of mangrove forests is shown to be as important as frictional effects in attenuating storm surge
- Reduction in peak storm surge level increases non-linearly as mangrove forest width (cross-shore) increases

Supporting Information:
- Supporting Information S1

Correspondence to:
J. M. Montgomery,
jmontgom31@gmail.com

Citation:
Montgomery, J. M., Bryan, K. R., Mullarney, J. C., & Horstman, E. M. (2019). Attenuation of storm surges by coastal mangroves. *Geophysical Research Letters*, *46*, 2680–2689. https://doi.org/10.1029/2018GL081636

Received 10 DEC 2018
Accepted 28 JAN 2019
Accepted article online 1 FEB 2019
Published online 11 MAR 2019

©2019. American Geophysical Union. All Rights Reserved.

Abstract The interaction between mangroves and storm surges is explored using an analytical solution. A simplified momentum equation, balancing vegetation drag and pressure gradient, is combined with the continuity equation resulting in a diffusion equation. Assuming a simplified environment, a one-dimensional analytical solution is obtained to predict peak surge level across a forest. The solution accurately reproduces peak water level of a 10-year return period flood event in mangroves in the Firth of Thames, New Zealand, and in Ten Thousand Islands, Florida, during Hurricane Charley. Vegetation properties that determine the capacity of mangroves to reduce surges are forest density and cross-shore extent. Storm characteristics—flood duration and peak water level at the forest fringe—also influence surge attenuation. Mangroves are shown to be an effective form of coastal flood protection if forests are sufficiently wide/dense, relative to the surge decay length scale, to restrict water exchange during a storm.

Plain Language Summary Storm-driven flooding is a major hazard in low-lying coastal areas. Mangroves have previously been shown to provide effective coastal protection from storm waves. However, there is sparse evidence that mangroves reduce storm surge, which is the temporary increase in water level resulting from the combination of high winds and low atmospheric pressure during a weather event. Here we demonstrate that mangroves can reduce water flow and store water, thus helping to reduce peak surge water levels. We show that if forests are sufficiently wide, water levels within (and landward of) the mangroves are substantially lower than for a scenario in which mangroves are absent. The density of the vegetation, cross-shore extent of the forest, and characteristics of the surge (duration and amplitude) all influence water-level reduction in the forest.

1. Introduction

Tropical cyclones can be destructive and deadly events in which coastal flooding is one of the primary causes of damage and casualties. Climate-change-driven sea level rise, increased storm frequency, and greater storm intensity are expected to enhance devastation due to storm surges (Woodruff et al., 2013). Coastal mangroves have been shown to lessen the impact of coastal storms by reducing wind-generated waves, dissipating currents, stabilizing sediments, and decreasing storm surge levels (Guannel et al., 2015; Temmerman et al., 2013). Existing documentation of the protective services mangroves provide with respect to storm surge attenuation can be separated into three categories (McIvor et al., 2016): observations of water level (Krauss et al., 2009), numerical simulations (Zhang et al., 2012), and analysis of damage caused by storm surges at coasts with and without mangroves (Das & Vincent, 2009). Numerical models are not always well validated (Zhang et al., 2012), and are sensitive to the way in which vegetation is represented (Horstman et al., 2013). Conversely, field observations of flood attenuation through mangroves are limited in location and events (primarily describing hurricane impacts on the gulf coast of the United States). Without a clear theoretical framework, applying observed flood attenuation rates to other sites is problematic. Given the loss of lives and infrastructure associated with coastal flooding (Costanza et al., 2008) and the potential for vegetation to reduce flooding, better understanding of the interaction between storm surge and mangroves is critically needed.

Environmental characteristics, such as vegetation density, root and stem diameter, bathymetry, and inundation characteristics influence the capacity of mangroves to reduce flood water levels (Alongi, 2008), but interaction between parameters has not been well quantified. Previous numerical experiments have shown that the influence of mangrove forest width (cross-shore extent) on storm surge attenuation is nonlinear (significant attenuation of water levels occurred across the forest fringe but little attenuation occurred at further distances into the forest), and surges from slow moving long-duration storms were less effectively

attenuated than those from faster-moving shorter-duration events (Zhang et al., 2012). However, the physical mechanisms to explain the above results were not provided.

Storm surge propagation in mangrove forests is friction-dominated and is reasonably well described as a "zero-inertia" diffusive wave (Friedrichs & Madsen, 1992; LeBlond, 1978). We develop a simplified analytic approximation to the nonlinear diffusion equation to describe the interaction between storm surge and emergent vegetation. Here the analytic solution is applied to two extreme surge events in contrasting mangrove forests, a 10-year return period flood event in the Firth of Thames, New Zealand, and Hurricane Harvey in Ten Thousand Islands, Florida. Such analytical solutions provide efficient and accurate predictions of surge levels across a forest.

2. Study Sites

2.1. Firth of Thames, New Zealand

The Firth of Thames (FoT) is a shallow ~800-km^2 basin in the North Island of New Zealand with a monoculture of gray mangroves (*Avicennia marina* var. *australasica*) occupying much of the southern shore. Mangrove colonization began in the mid-1950s, with trees currently varying in height from 0.5 to 3.5 m. The site is relatively uniform in the longshore direction, allowing for the hydrodynamics to be reasonably simplified to a one-dimensional problem. The mangrove forest extends ~1 km seaward of a stop bank, designed to prevent flooding of the low-elevation farmland behind the mangroves (Lovelock et al., 2010). The mesotidal estuary is a moderately wave exposed area (typically <1 m) with a spring tidal range of 2.8 m and neap range of ~2 m. The upper vegetated flat (Figure 1c) is 0.1–0.2 m above mean high water spring tide resulting in infrequent inundation of the forest (Swales et al., 2015). Storm surges in the region rarely exceed 0.5 m (Bell et al., 2000). The forest has no significant channels, and therefore, we can assume that fluid transport is dominated by flow through the vegetation. Additionally, the low slope of the vegetated portion of the upper intertidal supports a zero-slope simplification (Figure 1c).

2.2. Ten Thousand Islands, Florida

Located on the Gulf of Mexico coast in Florida, Ten Thousand Islands (TTI) is part of a large mangrove estuary with multiple mangrove species (red, white, and black mangroves) up to 9 m in height (Pool et al., 1977). (No pneumatophore information is provided.) The study site is located landward of the outer islands and is composed of ~3 km of mangrove forests before transitioning to salt marsh (Krauss et al., 2009). Tides influence the outer portion of the forest, but do not penetrate into the salt marsh.

2.3. Field Observations

2.3.1. Firth of Thames, November 2016 Event

Observations of extreme water levels across the mangroves in the FoT were collected in November 2016. A series of nine pressure sensors were deployed along a cross-shore transect extending from the stop bank to the vegetated intertidal (Figures 1b and 1c). Station 1 is located just seaward of the vegetation. Stations 2–5 are in the first ~100 m of the mangrove forest and provide a high degree of spatial resolution across the gently sloping (1:125) mangrove fringe. The remaining stations are roughly equally spaced across the vegetated tidal flat between the fringe and the stop bank. A small channel exists just seaward of the stop bank and may influence the inundation pattern toward the back of the mangrove forest. A long-term water-level gauge was located to the northeast of the study area. Additional details on the instrumentation and data processing are presented in Montgomery et al. (2018).

In November 2016, unusual astronomical conditions combined to create the largest spring tide in 70 years. On 17 November, a storm contributed to the abnormal tidal amplitude to generate a local peak water level 2.36 m above mean sea level, which corresponds to a 10-year return period flood at the long-term water-level gauge near the study site. As the surge propagated across the study site, a decrease in amplitude as well as a temporal delay in peak water levels was evident (Figure 2a).

2.3.2. Ten Thousand Islands, Hurricane Charley

Hurricane Charley impacted South West Florida in August 2004. Water-level data were collected at a permanent tide gauge positioned in Faka Union Bay just outside the mangrove forest (Figure 2d), site #A in the mangrove forest ~2.3 km from the bay, site #B at a transition from mixed mangrove to salt marsh at a distance of ~3.2 km, site #C in a marsh 4.5 km from the bay, and site #D 5.5 km from Faka Union Bay in

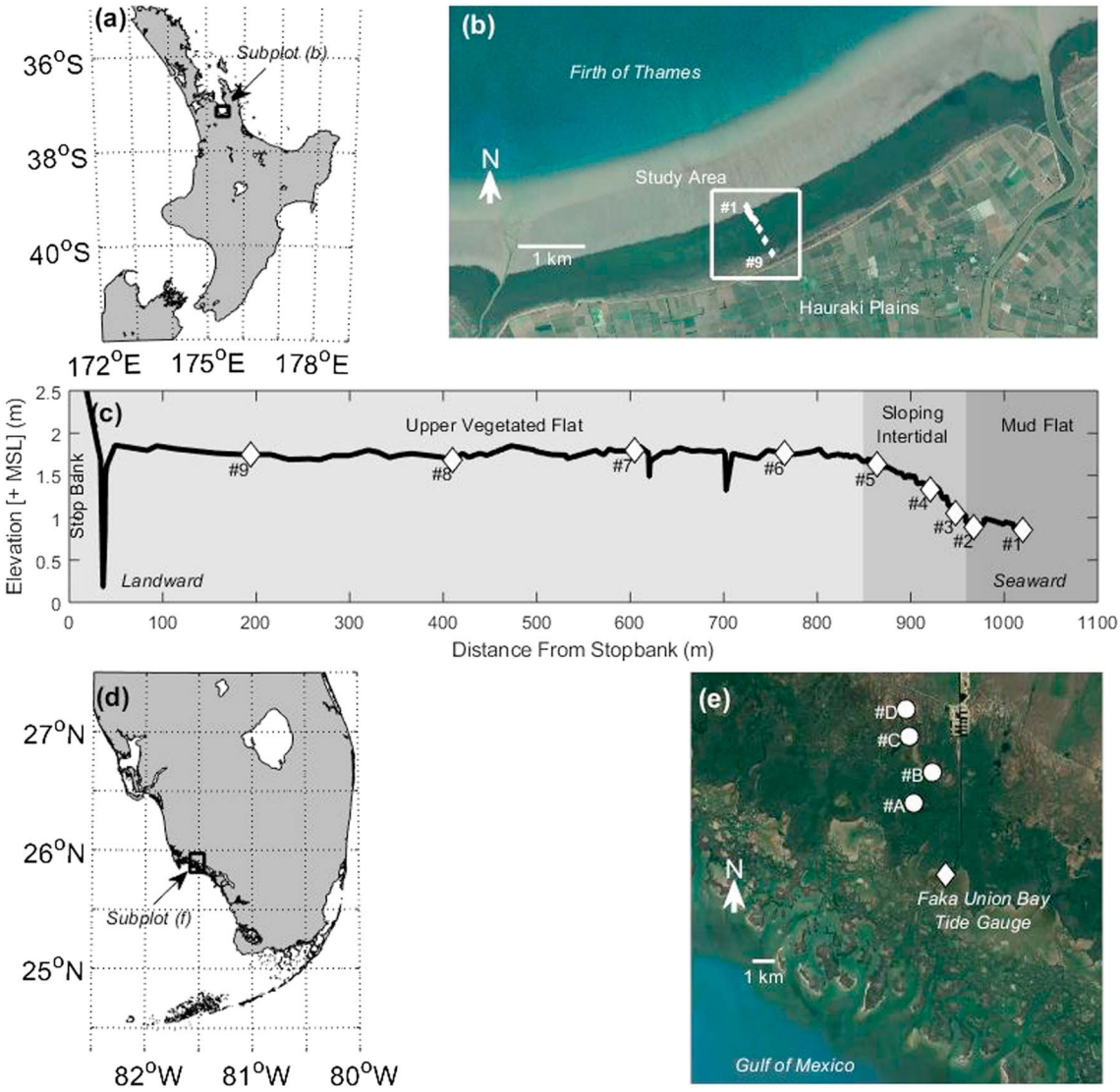

Figure 1. (a) North Island of New Zealand with the southern Firth of Thames (FoT) outlined in black. (b) FoT field study area (white) with instrument locations identified. (c) Location of instruments relative to stop bank in the FoT. (d) Florida with Ten Thousand Islands (TTI) study area (black). (e) Aerial image of TTI study site with instrument locations identified (photo sources: Google Earth).

a marsh (locations shown in Figure 1e). Note that no instrument elevations were recorded, and therefore, water levels cannot be related to a vertical datum; additional details on data collection and processing can be found in Krauss et al. (2009). The three most landward instrument sites were not influenced by tidal fluctuations, and therefore, storm surge height was determined by the difference between the 5-hr mean water level prior to the storm surge event and peak water level (Figure 2e). For tidally influenced instrument sites, storm surge height was determined as water level above predicted high tide.

3. Theoretical Model

Sheet flow over an intertidal platform with uniform vegetation cover contrasts with creek flow in which flow dynamics are dominated by transport through channels, and the higher elevation vegetated regions primarily act as water storage. A simple analytic solution to creek flow was previously developed (Friedrichs & Madsen, 1992). In contrast, the new formulation presented here characterizes a regime in which flux through flat vegetated areas dominates over flux through channels.

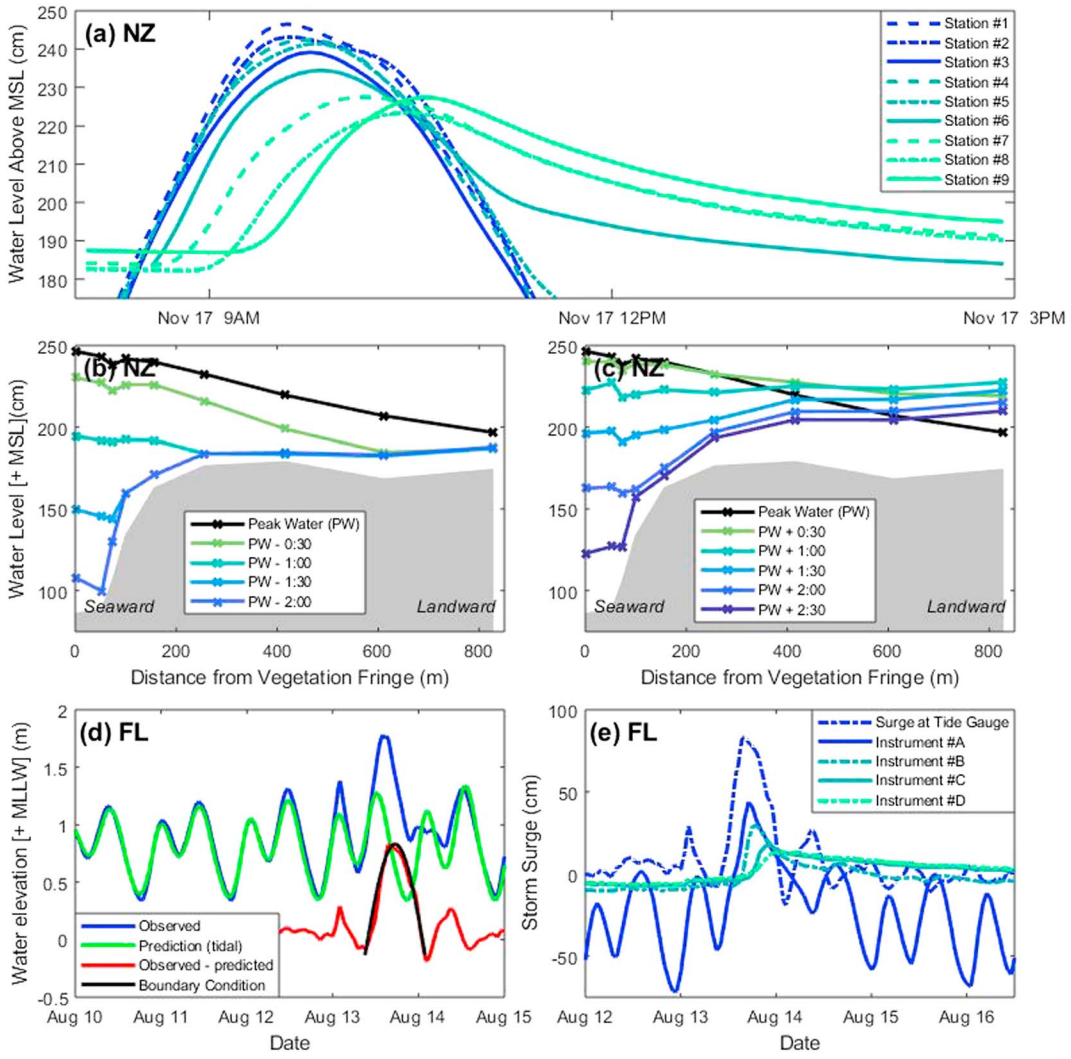

Figure 2. (a) Water levels at all nine instrument locations for surge event in the Firth of Thames (FoT). (b) Water levels along the FoT transect every 30 min (colors) before peak water level at the seaward boundary of the forest (black), data from surge event in panel (a). (c) Ebb water levels along the FoT transect every 30 min (colors) following the peak water level at seaward boundary of the forest (black). Note that maximum water level at the most landward station occurred 1 hr after peak water at the open boundary. (d) Ten Thousand Islands (TTI), Florida, 2004 Faka union tide gauge data (blue), tidal water-level prediction (green), difference between actual water level and predicted (red), and half sinusoid fit to represent boundary condition used in diffusion equation (black). (e) Storm surge water levels at instrument locations in TTI (colors). For the tidally influenced location (#A), storm surge is the difference between measured water level and average high tide level. For nontidal locations (#B, #C, #D), storm surge is calculated as the difference between measured water level and mean water level for the 5 hr prior to the surge event.

Sheet flow hydrodynamics through mangroves can be separated into three depth-dependent regimes imposed by the submerged portion of the plant. In shallow flows, friction is dominated by the high-density pneumatophores (aerial roots) which are typically between 5 and 25 cm in height (Horstman, et al., 2018). At intermediate water depths, flow interacts with trunks and pneumatophores. In sufficiently deep water, flow interacts with the canopy in addition to the trunks and pneumatophores. In the present work, flow past trunks and pneumatophores are examined, as water levels during the high-water events were not sufficient to be significantly influenced by the leafy canopy at these sites.

Long-period storm surge (~O (hours)) through uniform emergent vegetation is reasonably described by a simplified 1-D conservation of momentum equation (three-dimensional turbulence is parameterized by

vegetation drag, which is balanced by the pressure gradient). Combining momentum and continuity equations (see S1) yields a diffusion equation:

$$\frac{\partial \eta}{\partial t} = \frac{\partial}{\partial x}\left(D\frac{\partial \eta}{\partial x}\right), \tag{1}$$

where D is a nonlinear diffusion coefficient $D = h\sqrt{\frac{2g}{a_v C_D \frac{\partial \eta}{\partial x}}}$ which relates the temporal and spatial gradients of sea surface (η)—similar to Friedrichs and Madsen (1992), but assuming sheet flow (not channel flow) and that frictional drag is dominated by vegetation and not the seabed. Mangrove trunks are modeled as rigid emergent cylinders spaced sufficiently far apart for interelement interactions to be negligible (as suggested by Nepf (2004)). The diffusion coefficient D is a function of gravity g; drag coefficient C_d; water depth h, varying in both time and space; vegetation frontal area density a_v, varying in space and vertically with water depth; and spatial sea surface gradient $\frac{\partial \eta}{\partial x}$, varying in both time and space (Bedient & Huber, 1992). Note that larger water depths and lower vegetation density result in a larger diffusion coefficient and a greater rate of fluid exchange.

3.1. Constant Diffusion Coefficient Solution

An approximate analytic solution to equation (1) can be obtained by treating the diffusion coefficient D as a constant $\overline{\boldsymbol{D}}$ equal to the spatial and temporal average of the variable quantities (note that overbar designates a time average and angle brackets a spatial-average). The open boundary condition ($x = L$) is set by assuming a sinusoidally varying sea surface $\boldsymbol{\eta = a\ sin\ (\omega t)}$, with amplitude a and angular frequency $\boldsymbol{\omega}$ computed from fitting a half sine wave to the inundation event at the mangrove/open water interface. At the landward side of the basin ($x = 0$), a zero sea surface gradient boundary condition is assumed (associated with no flow through the boundary), providing the solution (following Friedrichs and Madsen (1992)):

$$\eta = a\,\frac{\cosh\left(\frac{x}{L_{\text{decay}}}\right)}{\cosh\left(\frac{L_{\text{forest}}}{L_{\text{decay}}}\right)}e^{i\omega t}; L_{\text{decay}} = \left(\frac{\overline{\langle D\rangle}}{i\omega}\right)^{1/2} = \left(\frac{\overline{\langle h\rangle} g^{1/2}}{i\omega\pi\left[2\langle a_v\rangle C_D\overline{\left\langle\frac{\partial \eta}{\partial x}\right\rangle}\right]^{1/2}}\right)^{1/2} \tag{2}$$

where sea surface elevation is dependent on the position in the basin x relative to the landward end of the forest, and the relationship between decay length scale L_{decay} and width of the mangrove forest L_{forest}.

Evaluating the decay length scale requires an estimate for average sea surface slope (averaged in both time and space), which was obtained by taking the time-averaged partial derivative of equation (2) evaluated at the open boundary ($x = L_{\text{forest}}$; Friedrichs & Madsen, 1992) to yield

$$\left|L_{\text{decay}}\right| = \left(\frac{\pi g\overline{\langle h\rangle}^2}{\omega^2 a_v C_D a\left|\tanh\left(\frac{L_{\text{forest}}}{L_{\text{decay}}}\right)\right|}\right)^{1/3}. \tag{3}$$

Equation (3) can be solved iteratively and requires an estimate for inundation period to obtain a value for angular frequency ω. To accommodate exposure at low tide in a solution that assumes a sinusoidal water-level boundary condition at the seaward end of the vegetation, a wave period of double the inundation duration was assumed. Amplitude a was set as the maximum water elevation above the seabed at the open boundary and average depth $\overline{h}$ as half that amplitude. Forest width L_{forest} and average vegetation frontal density a_v are assigned from field observations. Coefficient of drag C_d is ~1 for Reynolds numbers ≥200, with an average stem diameter of ~2 cm; this corresponds to velocities greater than 1 cm/s and indicates that flow through mangroves is often turbulent (Mullarney & Henderson, 2018). A more direct equation for decay length scale is obtained by rearranging equation (3), substituting, and simplifying, to obtain

$$|L_{\text{decay}}| = \left(\frac{gT^2 a}{16\pi \langle a_v \rangle \tanh\left(\frac{L_{\text{forest}}}{L_{\text{decay}}}\right)} \right)^{1/3}. \quad (4)$$

LeBlond (1978) originally proposed a diffusion equation to describe bottom friction-dominated tidal flows. A formulation for drag due to rigid emergent vegetation (suggested by Nepf (2004)) results in a different formulation for the diffusion coefficient compared to bottom friction dominated flows. The new equation presented here uses representative values to approximate variable quantities in the diffusion coefficient (similar to the methods of Friedrichs and Madsen (1992) for bottom friction dominated environments) to obtain an analytic solution to the nonlinear diffusion equation describing flooding through mangrove vegetation.

Depth-averaged flow velocities u can be found from the combination of the continuity equation and the time derivative of the solution to the diffusion equation (2) (Friedrichs & Madsen, 1992):

$$u = -\frac{ia\omega L_{\text{decay}}}{h_0} \frac{\sinh\left(\frac{x}{L_{\text{decay}}}\right)}{\cosh\left(\frac{L}{L_{\text{decay}}}\right)} e^{i\omega t}. \quad (5)$$

Flow speeds (not shown) are therefore greatest at the seaward edge of the vegetation ($x = L_{\text{forest}}$) and approach zero at the landward boundary ($x = 0$).

Alternative analytic approximations to friction-dominated flow such as Dronkers' (2005) linearization of the friction term are not appropriate in this case as, in strongly dissipative environments, drag is highly nonlinear (Lanzoni & Seminara, 1998).

3.2. Importance of Flow Through Pneumatophores

Baptist et al. (2007) described the time-averaged flow over submerged vegetation as being composed of four zones: a zone influenced by the bottom, flow through vegetation, a transition region at the top of the vegetation, and logarithmic flow above the vegetation. Our situation is reasonably described as a zone influenced by the bottom and two layers of vegetation: a submerged pneumatophore layer and an emergent trunk layer. Pneumatophore heights are variable and the gradual decline of vegetation density along the vertical diffuses the transition layer (Horstman, et al., 2018). Bed roughness is insignificant compared to the roughness provided by the dense pneumatophore cover (Horstman, et al., 2018), and therefore, influence of the bottom on water flux is ignored.

The relative importance of water flux through the pneumatophore and trunk layers can be examined by considering the ratio of discharge per unit width. Vegetation surveys in the FoT showed average pneumatophore densities ~2 m^{-1} with an average height of 0.1 m. Additionally, an average value for trunk frontal area density of 0.13 m^{-1} was found, although with substantial variability (values from 0.03 to 0.35 m^{-1}).

The ratio of the discharge through the pneumatophore zone and through the remainder of the water column can be obtained by solving for water velocity in equation (5) and using a simple formula for discharge per unit width $Q = u^*h$. The relative flow through pneumatophores is expressed as equation (6) below, with height of the pneumatophore layer and remaining water column (above the pneumatophores) denoted by h_P and h_T, respectively, and frontal area of the pneumatophores and trunks as a_P and a_T,

$$\frac{Q_P}{Q_T} = \frac{{a_T}^{1/2} h_P}{(a_T + a_P)^{1/2} h_T}. \quad (6)$$

The relative contribution of volume transported through the pneumatophore layer depends on total water depth and vegetation characteristics. FoT peak water depths reached 72 cm above the intertidal flat; therefore, for average vegetation parameters in the FoT, water flux through the pneumatophore layer is at least an order of magnitude lower than through the trunk zone, and so can reasonably be neglected. In the absence of further data, the same assumptions are applied to the TTI site.

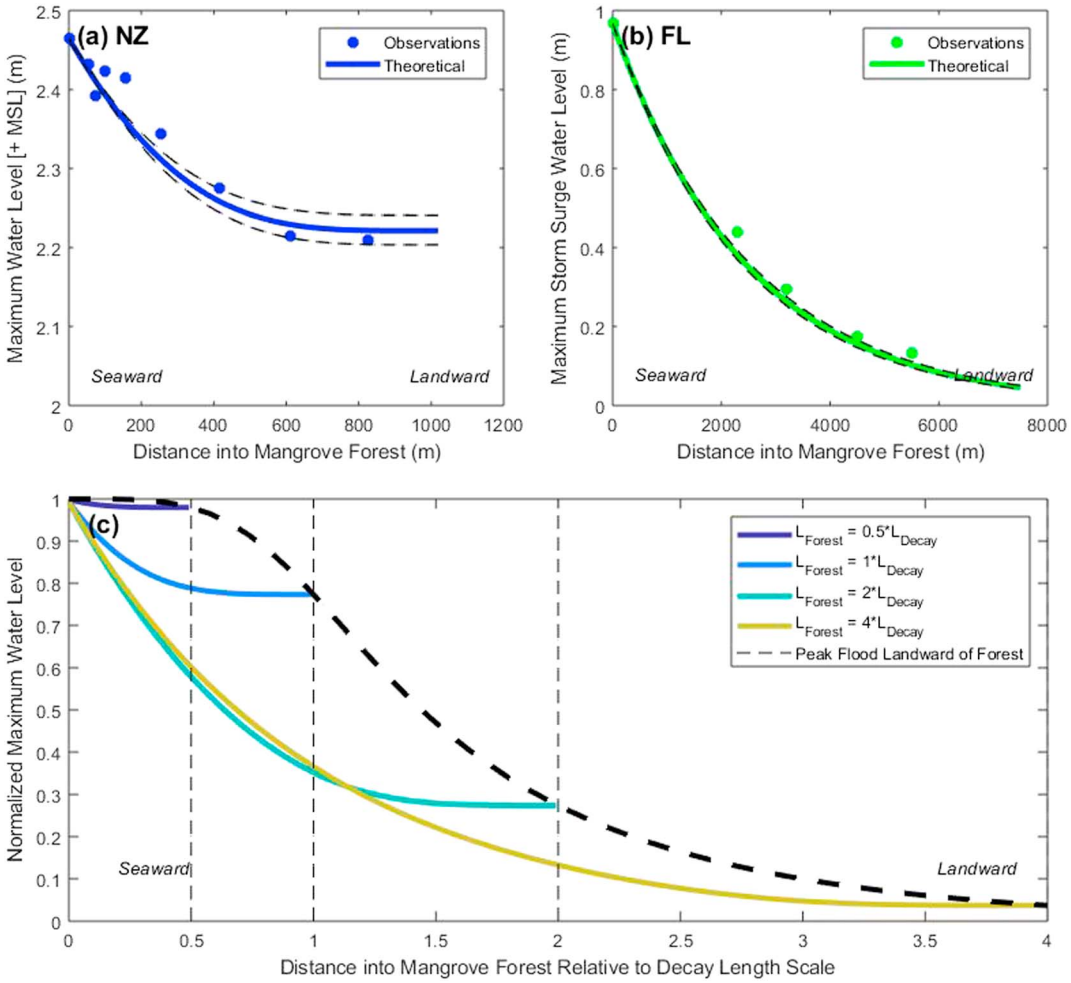

Figure 3. (a) Maximum water level predicted by the diffusion model (solid) and measured maximum water levels (dots) across the mangrove in FoT for November 2016 flood event shown in Figures 2a–2c (see text for details). (b) Maximum water level predicted by the diffusion model (solid) and measured maximum water levels (dots) across the mangrove forest in TTI for hurricane Charley (Figures 2d and 2e). Black dashed lines in (a) and (b) show the sensitivity to ±10% in a_v. (c) Decay of normalized maximum inundation level for different widths of mangrove forests (L_{forest}), normalized by inundation decay length scale (L_{decay}; solid). Dashed line shows total water level decay across mangrove forest widths.

4. Comparison of Model Predictions to Field Observations

4.1. Firth of Thames

Predicted maximum water levels across the FoT intertidal (equation (2))) were compared to observations (Figure 3a). Root-mean-square error between the theoretical model and observations is 2.7 cm. Flood duration and amplitude, used to establish the open water boundary condition, were selected from inspection of the flood signal of the most seaward instrument and estimated with respect to the top of the pneumatophore layer. Inundation duration of the flood event was 3 hr, 5 min and amplitude 0.62 m (above pneumatophore layer at ~1.85 m + mean sea level). Note that due to the sinusoidal forcing assumption, the period of the boundary condition signal is double the measured inundation duration. Mangrove properties were averaged over the study site, and a vegetation frontal area density of 0.13 m^{-1} was used for model computations; the real component of the resultant decay length scale is 812 m. Maximum flood water level decays most rapidly across the outermost vegetated region where maximum sea surface slope and therefore maximum flow speeds occur.

4.2. Ten Thousand Islands

Maximum water levels in the TTI mangroves predicted by the diffusion method showed strong agreement with observed peak water levels during Hurricane Charley (Figure 3b), with root-mean-square error

between the theoretical model and observations of peak water level of 3.6 cm. Forest fringe boundary conditions were selected from fitting a half sinusoid to the skew surge at the Faka Union tide gauge (Figure 2d), an inundation duration of 16 hr, 48 min and peak elevation of 0.97 m was identified. Due to a small local topographic gradient, no limit on forest width was imposed when calculating decay length of the flood signal (equation (4); $\tanh\left(\frac{L_{\text{forest}}}{L_{\text{decay}}}\right)\sim 1$). Mangrove frontal area of 0.19 m^{-1} was used in the diffusion model and was calculated from vegetation data presented by Pool et al. (1977) for the TTI site. The real component of the inundation decay length L_{decay} of Hurricane Charley through the TTI site is 2,460 m.

5. Discussion

Our solution to friction-dominated surge propagation through uniform mangroves has two parts: the formulation of decay length scale and the relationship between decay length scale and forest width. Decay length (equation (4)) increases with longer surge duration, deeper surge events, and less dense vegetation. Surge durations typically vary from a few hours, for fast-moving storms or tidally dominated inundation (as in FoT), to several days for large slow-moving events (Hurricane Harvey elevated water levels off the Gulf Coast of Texas for approximately four days). The variation in surge period is the dominant influence on decay length scale (changing by ~1 order of magnitude). Pool et al. (1977) presented mangrove density data for a variety of mangrove species in around 20 forests. Frontal area density of trunks and stems varied by ~1 order of magnitude (0.07–0.62 m^{-1}), influencing surge decay length by a factor of ~2. Observations by Zhang et al. (2012) showed that peak water levels of longer-duration hurricanes in South Florida were attenuated less than shorter-duration surges. Mangroves restrict the flow of water through the forest; therefore, shorter-period storms are unable to transport water through the forest as efficiently as longer-period storms, resulting in greater surge attenuation of shorter-duration events. In sufficiently long-duration floods, no attenuation of water level occurs and flood levels across the forest are uniform (e.g., narrow forest in Figure 3c).

The dynamics of storm surge through coastal mangroves are dependent on the relationship between inundation decay length and mangrove forest width (equation (3) and Figure 3c), as derived from the diffusion equation. Figure 3c shows the rate of decay of water level for a series of forests of varying relative length. Peak water level decays more rapidly in wider forests than in narrower, a result which can be attributed to additional water storage within the wider forest and the associated water flux through the vegetation. Although water level is not reduced as effectively in narrow forests, these results were generated assuming no water was transported landward of the inner forest boundary (further attenuation could occur if water storage exists landward of the vegetation). In the simplified environment assumed for this study, the outer portion of the vegetation acts to limit water exchange and the inner portion of the forest primarily serves as water storage, rendering the presence/properties of vegetation in the landward portion of the forest irrelevant. The forest in TTI was ~3.2 km wide with marsh landward of the mangroves. The rigid vegetation diffusion model with constant vegetation density (which only represents the front region of the wetland) accurately predicted water levels because the marsh landward of the mangroves acted only as water storage. Examining overall water-level reduction across mangrove forests shows that total attenuation of water level increases most rapidly (with additional forest width) when the decay length scale and forest width are approximately equivalent (slope of dashed line, Figure 3c). With sufficient forest width relative to the decay length of the surge event, mangroves effectively attenuate water levels by limiting fluid exchange across the forest.

Rigid emergent vegetation, dominated by sheet flow, is assumed in our new adaptation of (Friedrichs & Madsen, 1992), and therefore, our method is not applicable to a wider array of coastal vegetation or geomorphology. The flexibility of saltmarsh grasses invalidates the assumption that the drag coefficient is independent of velocity and that vegetation frontal area is only proportional to depth (reviewed in Nepf, 2012; Mullarney & Henderson, 2018). Saltmarshes are likely to be fully submerged during extreme events and the dominant water transport mechanism will either be through channels or skimming above the submerged vegetation. Application of the diffusion method requires a single frontal area value to be representative of the flow impeding effect of vegetation. Therefore, model application depends on mangroves being distributed such that flow routing through channels, around patches, or over submerged vegetation is insignificant, and sufficiently rigid to not deflect in flow. Moreover, the method assumes the momentum

balance is characterized by sea surface gradient and friction due to emergent vegetation. Tsunamis and very large/short-duration storm surges may require additional terms in the momentum equation.

5.1. Variations in the Diffusion Coefficient

The assumption of a constant diffusion coefficient facilitated an analytic solution to the diffusion equation, but results in symmetrical surge waves. The diffusion coefficient (equation (3)) contains three sources of variation: linear dependence on water depth (η), nonlinear dependences on sea surface slope $\left(\frac{\partial \eta}{\partial x}\right)$, and dependence on vegetation characteristics (a_v). The emergent vegetation assumption provides a linear relationship between the diffusion coefficient and depth (equation (1)). The upper portion of the surge propagates at higher velocity than the lower portion resulting in a flood-dominant asymmetry, shorter flood stage, and longer ebb stage (Parker, 1984), which is not captured by a constant diffusion coefficient. Although vegetation reduces peak surge levels due to limiting water exchange, vegetation also reduces the rate at which water returns to the seaward boundary, increasing ponding time (Figures 2a and 2e; Rodríguez et al., 2017). The constant diffusion coefficient solution produces a decaying, temporally shifted sine wave that overpredicts the rate of the receding water levels. The depth dependence of the diffusion coefficient is of greater importance in a traditional bottom friction-dominated environment ($D \sim \eta^{5/3}$ (Friedrichs & Madsen, 1992)) than for the linear dependence in emergent vegetation presented here.

Vertical and horizontal variations in vegetation induce complexity in flow that is not captured by the present approach. Mangrove trunk densities varied up to an order of magnitude throughout the FoT study area. Despite this variation, the simplified solution assuming uniform mangrove density well matched observations (Figure 3a). The vegetation variations were not organized in patches and did not cause significant flow routing; therefore, averaging mangrove characteristics resulted in a representative value for estimating drag due to vegetation. Highly channelized and creek dissected mangroves do not attenuate surge water levels as effectively as more uniform forests without creeks (Krauss et al., 2009; Montgomery et al., 2018).

6. Conclusions

Surge propagation in a friction-dominated mangrove environment is well described as a diffusive phenomenon. Mangrove forests have been conceptualized here as a buffer limiting water exchange and providing water storage. Our new analytic solution derived from the linearized diffusive model compared well with field observations of extreme surges in two contrasting mangrove environments. Mangroves have been shown to provide effective coastal flood protection if forests are sufficiently wide with respect to the decay length scale of the surge wave. The newly derived simplified equations that isolate the dominant physics can be helpful in both qualitatively and quantitatively understanding surge attenuation in mangrove forests and provide an easily accessible solution without the need for advanced computing resources. Such formulae can help with planning for sea level rise and flooding scenarios in the vulnerable low-lying areas that characterize many tropical and subtropical coastlines.

Acknowledgments
The research presented was supported by the Natural Hazards Platform (contract C05X0907). K.R.B., J.C.M., E.M.H., and the field work were funded by the Marsden Fund (grant 14-UOW-011). The authors acknowledge the field help provided by Caitlyn Gillard, Hieu Nguyen, Dave Culliford, and Rex Fairweather. Montgomery, John. (2018). Mangrove Field Study, Firth of Thames New Zealand, November 2016 (Version 1) [Data set]. Zenodo doi: 10.5281/zenodo.1323413 Montgomery, John. (2018). Mangrove Water Level Study, Tauranga New Zealand (Version 1) [Data set]. Zenodo. doi: 10.5281/zenodo.1323417.

References

Alongi, D. M. (2008). Mangrove forests: Resilience, protection from tsunamis, and responses to global climate change. *Estuarine, Coastal and Shelf Science*, *76*, 1–13. https://doi.org/10.1016/j.ecss.2007.08.024

Baptist, M. J., Babovic, V., Rodríguez Uthurburu, J., Keijzer, M., Uittenbogaard, R. E., Mynett, A., & Verwey, A. (2007). On inducing equations for vegetation resistance. *Journal of Hydraulic Research*, *45*, 435–450. https://doi.org/10.1080/00221686.2007.9521778

Bedient, P. B., & Huber, W. C. (1992). *Hydrology and Floodplain Analysis* (2nd ed.). Reading, MA: Addison-Wesley.

Bell, R. G., Goring, D., & de Lange, W. P. (2000). Sea-level change and storm surges in the context of climate change. *Transactions of the Institution of Professional Engineers New Zealand: General Section*, *27*(1), 1.

Costanza, R., Pérez-Maqueo, O., Martinez, M. L., Sutton, P., Anderson, S. J., & Mulder, K. (2008). The value of coastal wetlands for hurricane protection. *Ambio: A Journal of the Human Environment*, *37*, 241–248. https://doi.org/10.1579/0044-7447(2008)37[241:TVOCWF]2.0.CO;2

Das, S., & Vincent, J. R. (2009). Mangroves protected villages and reduced death toll during Indian super cyclone. *Proceedings of the National Academy of Sciences*, *106*, 7357–7360. https://doi.org/10.1073/pnas.0810440106

Dronkers, J. J. (2005). *Dynamics of Coastal Systems* (Vol. 25). Hackensack: World Scientific Publishing Company.

Friedrichs, C. T., & Madsen, O. S. (1992). Nonlinear diffusion of the tidal signal in frictionally dominated embayments. *Journal of Geophysical Research*, *97*(C4), 5637–5650. https://doi.org/10.1029/92JC00354

Guannel, G., Ruggiero, P., Faries, J., Arkema, K., Pinsky, M., Gelfenbaum, G., et al. (2015). Integrated modeling framework to quantify the coastal protection services supplied by vegetation. *Journal of Geophysical Research: Oceans*, *120*, 324–345. https://doi.org/10.1002/2014JC009821

Horstman, E. M., Bryan, K. R., Mullarney, J. C., Pilditch, C. A., & Eager, C. A. (2018). Are flow-vegetation interactions well represented by mimics? A case study of mangrove pneumatophores. *Advances in Water Resources*, *111*, 360–371. https://doi.org/10.1016/j.advwatres.2017.11.018

Horstman, E. M., Dohmen-Janssen, C. M., & Hulscher, S. J. M. H. (2013). Modeling tidal dynamics on a mangrove creek catchment in Delft3D. Paper presented at the Coastal Dynamics, Arcachon, France.

Krauss, K. W., Doyle, T. W., Doyle, T. J., Swarzenski, C. M., From, A. S., Day, R. H., & Conner, W. H. (2009). Water level observations in mangrove swamps during two hurricanes in Florida. *Wetlands*, *29*, 142–149. https://doi.org/10.1672/07-232.1

Lanzoni, S., & Seminara, G. (1998). On tide propagation in convergent estuaries. *Journal of Geophysical Research*, *103*(C13), 30,793–30,812. https://doi.org/10.1029/1998JC900015

LeBlond, P. H. (1978). On tidal propagation in shallow rivers. *Journal of Geophysical Research*, *83*(C9), 4717–4721. https://doi.org/10.1029/JC083iC09p04717

Lovelock, C. E., Sorrell, B. K., Hancock, N., Hua, Q., & Swales, A. (2010). Mangrove forest and soil development on a rapidly accreting shore in New Zealand. *Ecosystems*, *13*(3), 437–451. https://doi.org/10.1007/s10021-010-9329-2

McIvor, A., Spencer, T., Möller, I., & Spaldinga, M. (2016). 2|Coastal defense services provided by mangroves. *Managing Coasts with Natural Solutions*, 24.

Montgomery, J., Bryan, K., Horstman, E., & Mullarney, J. (2018). Attenuation of tides and surges by mangroves: Contrasting case studies from New Zealand. *Water*, *10*, 1119. https://doi.org/10.3390/w10091119

Mullarney, J. C., & Henderson, S. M. (2018). Flows within marine vegetaion canopies. In V. Panchange & J. Kaihatu (Eds.), *Advances in Coastal Hydraulics* (pp. 1–46). Hackensack: World Scientific Publishing Ltd. https://doi.org/10.1142/9789813231283_0001

Nepf, H. (2004). Vegetated flow dynamics. In *The Ecogeomorphology of Tidal Marshes* (pp. 137–163). Washington, DC: American Geophysical Union. https://doi.org/10.1029/59CE09

Nepf, H. (2012). Hydrodynamics of vegetated channels. *Journal of Hydraulic Research*, *50*(3), 262–279. https://doi.org/10.1080/00221686.2012.696559

Parker, B. B. (1984). Frictional effects on the tidal dynamics of a shallow estuary. (PhD thesis). Balitmore, MD: Johns Hopkins University.

Pool, D. J., Snedaker, S. C., & Lugo, A. E. (1977). Structure of mangrove forests in Florida, Puerto Rico, Mexico, and Costa Rica. *Biotropica*, *9*(3), 195–212. https://doi.org/10.2307/2387881

Rodríguez, J. F., Saco, P. M., Sandi, S., Saintilan, N., & Riccardi, G. (2017). Potential increase in coastal wetland vulnerability to sea-level rise suggested by considering hydrodynamic attenuation effects. *Nature Communications*, *8*, 16094. https://doi.org/10.1038/ncomms16094

Swales, A., Bentley, S. J., & Lovelock, C. E. (2015). Mangrove-forest evolution in a sediment-rich estuarine system: Opportunists or agents of geomorphic change? *Earth Surface Processes and Landforms*, *40*, 1672–1687. https://doi.org/10.1002/esp.3759

Temmerman, S., Meire, P., Bouma, T. J., Herman, P., Ysebaert, T., & De Vriend, H. J. (2013). Ecosystem-based coastal defence in the face of global change. *Nature*, *504*, 79. https://doi.org/10.1038/nature12859–83.

Woodruff, J. D., Irish, J. L., & Camargo, S. J. (2013). Coastal flooding by tropical cyclones and sea-level rise. *Nature*, *504*, 44. https://doi.org/10.1038/nature12855–52.

Zhang, K., Liu, H., Li, Y., Xu, H., Shen, J., Rhome, J., & Smith, T. J. (2012). The role of mangroves in attenuating storm surges. *Estuarine, Coastal and Shelf Science*, *102-103*, 11–23. https://doi.org/10.1016/j.ecss.2012.02.021